Helena Mateos, Luigi Gentile, Sergio Murgia, Giuseppe Colafemmina, Mattia Collu, Johan Smets, Gerardo Palazzo,

Understanding the self-assembly of the polymeric drug solubilizer Soluplus®,

Journal of Colloid and Interface Science,

Volume 611,

2022,

Pages 224-234,

ISSN 0021-9797,

https://doi.org/10.1016/j.jcis.2021.12.016.

(https://www.sciencedirect.com/science/article/pii/S0021979721021445)

Understanding the self-assembly of the polymeric drug solubilizer Soluplus®

Helena Mateos,[a] Luigi Gentile, [a] Sergio Murgia,[b] Giuseppe Colafemmina, [a] Mattia Collu,[c] Johan Smets,[c] Gerardo Palazzo* [a]

[a] Dipartimento di Chimica, Università di Bari "Aldo Moro" & CSGI (Consorzio per lo Sviluppo dei Sistemi a Grande Interfase), Via Orabona 4, Bari, I-70126, Italy
[b] Dipartimento di Scienze della Vita e dell'Ambiente, Università degli Studi di Cagliari & CSGI (Consorzio per lo Sviluppo dei Sistemi a Grande Interfase), via Ospedale 72, Cagliari, 09124, Italy
[c] The Procter & Gamble Company, Temselaan 100, 1853 Strombeek Bever, Belgium

*Correspondence to: gerardo.palazzo@uniba.it tel: +39-338-3841217

E-Mail addresses of co-authors:
Helena Mateos: helena.mateos@uniba.it;
Luigi Gentile: luigi.gentile@uniba.it;
Sergio Murgia: murgias@unica.it;
Giuseppe Colafemmina: giuseppe.colafemmina@uniba.it;
Mattia Collu: collu.m@pg.com;
Johan Smets: smets.j@pg.com

ABSTRACT

Hypothesis: Soluplus® is one of the most widely used amphiphilic copolymers in drug delivery and has been reported to strongly enhance the adsorption of model drugs. However, there is still a limited understanding of its micellar behavior as it responds to the different routes of administration, which involve important changes in concentration.

Experiments: The microstructure of Soluplus aqueous solutions has been investigated at a wide range of polymer concentrations ($2x10^{-6}$ – 0.2 g/mL) by a combination of diffusion NMR (dNMR), small angle X-ray scattering (SAXS), static (SLS) dynamic (DLS) light scattering and viscosity measurements. These techniques have been coupled with surface tension measurements to frame the polymer's critical micellar concentration (cmc).

Findings: We demonstrate the presence at all tested concentrations of two forms of Soluplus, with hydrodynamic radii of 3 and 26 nm, where the fraction of smaller objects accounts for as much as 60-70%. dNMR, SAXS, DLS and SLS indicate that Soluplus spontaneously self-assembles into large spherical particles with a core-shell structure. However, self-assembly takes place three orders of magnitude above the cmc evaluated via surface tension measurements. Instead of the traditional cooperative micellization process, we propose a thermal-activated isodesmic self-assembly of the small aggregates into core-shell micelles.

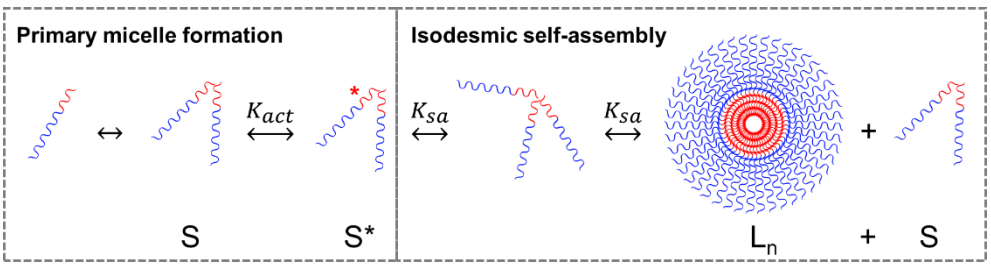

Keywords: Polymeric micelles, isodesmic self-assembly, diffusion NMR, light scattering, small angle X-ray scattering (SAXS), hard spheres interactions

1. Introduction

The pharmaceutical industry is progressing towards actives with increasing molecular weights and poor water solubility, lowering the absorption by the body and challenging their delivery. [1] This general trend is pushing toward approaches to improve apparent solubility and oral bioavailability while maintaining a stable amorphous state during shelf life and sustaining supersaturation during drug release.

Nanosystems are one of the current, most attractive approaches for different issues related to drug delivery. Nanocarriers play an important role in the improvement of pharmaceutical ingredients solubility and stabilization of easily degradable compounds.[2] Amphiphilic polymers are able of self-assembling into micelles with an external hydrophilic shell and a hydrophobic core that eases the solubilization and protects insoluble hydrophobic drugs.[3–5] In the recent past there is a growing tendency towards the use of polymeric surfactants as carriers in solid dispersion technology.[6] For example, according to WoS©, in the last 5 years more than 1000 papers are being published every year in the topic of polymeric micelles.[7] One important advantage of using micelles as a strategy for drug delivery is their relatively small size (usually <100nm) compared to other nanocarriers and to the dimension of the pores in the body's vasculatures.[8] Consequently, enabling a more efficient blood circulation, tissue penetration and cellular internalization.[9–13]

However, a key limitation to the use of micelles for drug delivery resides in their low resilience to changes in their environment. When micelle formulations are injected or orally administered, they get diluted, which can get to dissociation if the concentration falls below the polymer's cmc. If not carefully controlled, this micelle disintegration can lead to a prompt release of the encapsulated drug leading to a series of drawbacks such as poor or variable adsorption, low targeting capability or high drug loading.[14] On the other hand, if properly designed, these changes in stability with changes in the environment can be used to control drug release, such as the widely used pH-sensitive polymeric micelles.[15]

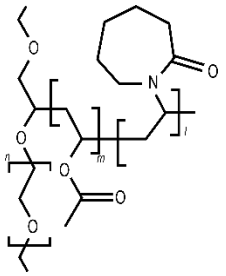

Figure 1. Molecular structure of Soluplus.

In this paper we have investigated the behaviour of one of the most extensively used non-ionic amphiphilic polymers for drug delivery applications: Soluplus®. Soluplus® consists of a polyethylene glycol (PEG 6000) backbone grafted with one or two randomly copolymerized polyvinyl caprolactam–polyvinyl acetate side chains (see Fig.1).[6]

This polymer shows a significant improvement of the solubility of hydrophobic pharmaceutical ingredients [16–19] and has been proposed as a carrier in oral drug delivery, [17,18,20,21] ocular, [22,23] and topical delivery, [24–26] in intravenous injection for cancer treatment, [19,27] or as a novel adjuvant for vaccine delivery in transcutaneous immunization of tetanus toxoid. [28]

Previous studies on Soluplus put emphasis on its interaction with drugs rather than on its behaviour in solid [1,16,18,29–31] and aqueous solution. [17,19,27,28,32,33] Notwithstanding its wide range of use, a systematic study on the properties of aqueous Soluplus solutions could be the key for the development of more efficient drug delivery systems. In this work, a wide range of Soluplus aqueous concentrations ($2x10^{-6}$ – 0.2 g/mL) has been studied with the aim of evaluating the solubilization mechanisms of Soluplus covering concentrations below and above the cmc values found in literature ($8x10^{-6}$[19,34] -$8x10^{-4}$ g/mL[20] [32]) and the higher Soluplus concentrations that are often used in formulations (0.02- 0.2 g/mL).

More specifically, we have studied the aggregation mechanism combining surface tension and viscosity measurements with static and dynamic light scattering measurements. These, combined with diffusion NMR and small angle X-ray scattering experiments allow for a complete image of the aggregation mechanism of Soluplus in aqueous media.

2. Material and methods

2.1. Light scattering measurements

Nanosizer ZS (Malvern instruments) was used for the Static Light Scattering (SLS) and Dynamic Light Scattering (DLS) measurements at 25°C in quartz rectangular cuvettes. Light scattering experiments were performed in backscattering at a fixed detector angle of 173°. DLS data were collected leaving the instrument free to optimize the instrumental parameters (attenuator, optics position and number of runs). The time autocorrelation function (ACF) of scattered light intensity was taken as the average of 10-12 consecutive runs of 10 s each. For a monodisperse sample, the ACF decays exponentially with the autocorrelation time, τ, as

$$ACF = \beta \cdot \exp(-D_m q^2 \tau) \qquad (1)$$

where $\beta \sim 1$ is the spatial coherence factor, $q = \frac{4\pi n}{\lambda} \sin\frac{\theta}{2}$ is the modulus of the scattering vector depending on the scattering angle θ, the laser wavelength λ and the solution refractive index n. D_m is the mutual diffusion coefficient reflecting the relaxation rate of the concentration fluctuations (on a length-scale $2\pi/q$).

For SLS the intensity of light scattered by the sample (I), by the filtered solvent only (I_{solv}) and by the reference liquid toluene (I_{ref}) where measured using the same square quartz cell. The data were then converted into absolute scattering intensities, i.e. "excess Rayleigh ratios" ($\Delta\Re$) according to [35]

$$\Delta\Re(\theta) = \frac{I - I_{solv}}{I_{ref}} \Delta\Re_{ref} \left(\frac{n}{n_{ref}}\right)^2$$

where $\Delta\Re$ref= $14x10^{-6}$ cm^{-1} is the Rayleigh ratio of toluene at 633 nm, n and n_{ref} the refractive index of the solution and toluene, respectively, at the same wavelength. In the evaluation of n and for subsequent calculations an increment in the solution's refractive index of (dn/dC) = 0.15 cm^3/g was assumed (C is the weight concentration).

2.2. dNMR Measurements

In order to reduce the contribution of the water signal in the NMR spectra samples were prepared in D_2O.

^{1}H NMR diffusion measurements (dNMR) were carried out in a Bruker Avance 300 MHz (7.05 T) spectrometer at the operating frequency of 300.131. A standard BVT 3000 variable temperature control unit was used to set the temperature at 25 °C. Self-diffusion coefficients were determined using a Bruker DIFF30 probe supplied by a Bruker Great 1/40 amplifier that can generate field gradients up to 1.2 T m^{-1}. The pulse-gradient stimulated echo (PGSTE) sequence was used. Self-diffusion coefficients were obtained by varying the gradient strength (g) while keeping the gradient pulse length (δ) and the delay time (Δ) between the encoding and decoding gradients constant within each experimental run.

For monodisperse samples, the measured self-correlation function (SCF also called echo attenuation) obeys the Stejskal- Tanner equation: [36]

$$SCF = \frac{I}{I_0} = \exp(-D_s q^2 t) \qquad (2)$$

Where I and I_0 are the signal intensities in presence and absence of the applied field gradient, respectively. The term $q = \gamma g \delta$ is, formally, the modulus of a space vector defined by the duration, δ, and intensity, g, of the applied gradient pulse (γ being the gyromagnetic ratio of the observed nucleus), $t = (\Delta - \delta/3)$ is the actual diffusion time. In eq. 2 D_s is the self-diffusion coefficient reflecting the mean-square displacement per unit time associated to self-motion in an environment at constant concentration.

2.3 SAXS

Small-angle X-ray scattering measurements have been performed using the SAXSLab Ganesha 300XL instrument (SAXSLAB ApS, Skovlunde, Denmark), a pinhole collimated system equipped with a Genix 3D X-ray source (Xenocs SA, Sassenage, France). Data have been collected with the detector placed at two sample-to-detector distances yielding a *q*-region between 0.0042 and 0.48 Å^{-1}. q is the scattering vector, $q = (4\pi\sin(\theta/2))/\lambda$, where θ is the scattering angle and λ is the wavelength of 1.54 Å. The samples were sealed in a 1.5 mm diameter capillary. During the experiments the temperature was controlled by an external recirculating water bath with a temperature accuracy of 0.2 °C and kept constant at 25 °C. The two-dimensional (2D) scattering pattern was recorded using a 2D 300 k Pilatus detector (Dectris Ltd., Baden, Switzerland) and radially averaged using the SAXSGui software to obtain I(q). The scattering profile was obtained by subtracting the solvent (data acquired in the same capillary with the same exposure time) and the data was brought to absolute scale using water as a primary standard.

2.4 Surface tension and viscosity measurements

Surface tension of aqueous polymer solutions were measured at 25°C by the Du Noüy ring method using a Krüss K8600 tensiometer (Krüss GmbH, Hamburg, Germany). Measurements were taken after 30 min from mixing to ensure the adsorption equilibrium of Soluplus at the liquid interface. Each value was taken as the average of at least 3 replicates.

Viscosity measurements have been carried out using a vibrational viscometer SV-10 (A&D) at room temperature (25$\pm$1 °C). The natural frequency of the vibrating elements is 30 s^{-1}.

3. Results

3.1 Two-state distribution of Soluplus chains: low concentration

3.1.1 dNMR, DLS & SAXS

The echo attenuation (i.e. the self-correlation function or SCF) shown in Fig. 2A of Soluplus NMR signal (3.7 ppm) in solution at 0.011 g/mL, deviates unmistakably from a single exponential decay (eq. 2) as it is composed by a fast and a slow diffusing components which differ by at least one order of magnitude in diffusivity.

Accordingly, the SCF has been fitted to a sum of two decays [37]:

$$SCF = (1 - P_{slow})exp\left(-D_{fast}q^2\tau\right) + P_{slow}exp(-D_{slow}q^2\tau) \qquad (3)$$

Where P_{slow} is the fraction of polymer diffusing with the slow self-diffusion coefficient, D_{slow} and D_{fast} are the self-diffusion coefficients of the slow and fast diffusing polymer, respectively.

The results of such an analysis (listed in Table 1) indicate that a large fraction (68%) of the polymer is fast diffusing (D_{fast}= 6.6x10^{-11} m^{2}s^{-1}) while the remaining (P_{slow} = 0.32) diffuses with a diffusivity that is one order of magnitude lower (D_{slow}= 7.5x10^{-12} m^{2}s^{-1}). Being the concentration relatively low, an apparent hydrodynamic radius (r_h) can be calculated applying the Stokes-Einstein relation:

$$r_h = \frac{k_bT}{6\pi\eta D} \qquad (4)$$

Where D is the diffusion coefficient, η the solvent viscosity and k_bT is the thermal energy. Note that, strictly, eq. 4 holds only at infinite dilution. At finite concentration, interparticle and hydrodynamic interactions affect

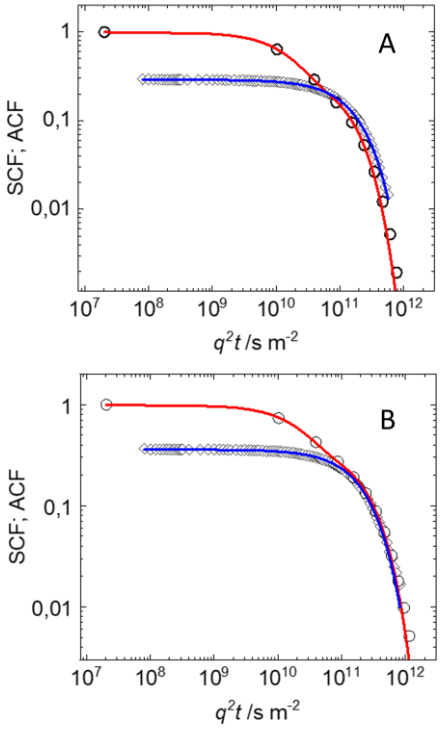

the diffusion coefficient and, in the absence of suitable corrections for such effects, the hydrodynamic radius

Figure 2. Comparison of the SCF (empty dots) and ACF (empty grey diamonds) obtained with dNMR and DLS respectively for 0.01 (A) and 0.062 g/mL (B) Soluplus solutions. The corresponding diffusivities obtained from the fittings are presented in Table 1.

evaluated directly from eq. 4 must be considered as an apparent size that is meaningful only at low concentrations. [38]

The application of eq. 4 to the fit of Fig. 2A reveals that Soluplus in solution stays on different sites with different hydrodynamic sizes. The fast-diffusing 68% of the polymer has an apparent hydrodynamic radius of 3.0 ± 0.1 nm while the remaining slow-diffusing 32% is present on aggregates with $r_h = 26 \pm 1$ nm. The latter is close to the size (35 nm) attributed (at room T), by means of DLS measurements, to Soluplus micelles in the few papers dealing with solution properties of this polymer. [24,39].

To gain insight on the apparent differences between diffusion measuring techniques, DLS measurements were performed on the very same samples measured with dNMR. When comparing dNMR and DLS, one must be aware of the fact that the contribution of 1H-dNMR SCF is weighted by the number of protons, while in DLS it depends on the intensity of scattered light, which scales as the square of the particle's mass. [38]

The mass, in turn, scales as $mass \propto R_g^{d_f}$ where R_g is the gyration radius and d_f is the fractal dimension (d_f =2 for random coil and d_f =3 for a compact particle). [40]

In the present case, since the fast-diffusing species have a size that is one order of magnitude smaller, their contribution to the scattering should be negligible (10^{-4} – 10^{-6}) compared to the larger ones. We anticipate here that in this system the hydrodynamic radii are close to the gyration radii. Accordingly, the DLS ACF can be fitted to a single exponential (eq. 1) with a (mutual) diffusion coefficient D_m= 5.47x10^{-12} m^2s^{-1}, close to the D_{slow} probed by dNMR.

The small discrepancy between D_m and D_{slow} is not surprising considering these quantities have different meanings but are expected to have mutually close values that coincide at infinite dilution only (for details see [38].

Table 1. Diffusion coefficients probed by dNMR and DLS for solutions of Soluplus in D_2O.

wt%	g/mL	D_{fast}/m^2s^{-1}	P_{slow}	D_{slow}/m^2s^{-1}	D_m/m^2s^{-1}
1	0.011	(6.6±0.2)x10^{-11}	0.32±0.01	(7.5±0.3)x10^{-12}	(5.5±0. 1)x10^{-12}
5.65	0.062	(4.6±0.2)x10^{-11}	0.39±0.01	(4.2±0.2)x10^{-12}	(4.4±0.2)x10^{-12}
10	0.109	(3.3±0.2)x10^{-11}	0.36±0.01	(2.1±0.2)x10^{-12}	(2. 8±0. 3)x10^{-12}
21.15	0.228	(1.5±0.5)x10^{-11}	0.51±0.01	(7.1±0.5)x10^{-13} σ=(5.1±0.1)x10^{-13}	(8.7±0.1)x10^{-13} σ=(7.1±0.1)x10^{-13}

For samples at 1, 5.65, 10 wt% the dNMR SCF have been fitted to eq. 10 and the DLS ACF have been fitted to eq. 1. For the sample at 21.15 wt% dNMR SCF has been fitted to eq. 17 (expanded to the IV-order cumulant) and the DLS ACF has been fitted to eq. 16 (expanded to the IV-order cumulant)

The SCF probed by dNMR and the ACF probed by DLS formally obey the same relationship (see eqs. 1 and 2 in the experimental section) and can be, therefore, plotted on the same graph using q^2t in s/m^2 as abscissa. This treatment has been applied in Fig. 2A where, for a fair comparison, the DLS ACF has been properly normalized to the contribution of the slow phase observed in the dNMR SCF (P_{slow}). Inspection of Fig. 2A reveals how the DLS ACF superimposes to the slow phase of the dNMR SCF.

An analogous behavior is observed for 0.062 g/mL Soluplus in D_2O. Also in this case, the DLS ACF accounts for the slow phase of the dNMR SCF (see Fig. 2B). The dNMR SCF is bi-exponential and fitting to eq. 3 gives a small slow-diffusing fraction (P_{slow} = 0.38) with a D_{slow} that is very close to the one measured by DLS (the best

fit values are listed in Table 1). The polymer concentration is here nonnegligible (the viscosity is 1.8 times that of water, *vide infra*) and, in the absence of a suitable model accounting for concentration effects, the evaluation of hydrodynamic sizes is useless.

The dNMR data unambiguously indicates the polymer is present in two forms that differ in hydrodynamic size, the larger being likely the Soluplus micelles defined in literature and that have also been evidenced by conventional TEM [17,39]. It is surprising that the fraction with smallest hydrodynamic size is the large majority (above 60%) of the polymer even when 0.01 g/mL is almost three orders of magnitude above the cmc.

SAXS measurements were performed, on a wide angular range, to shed some light on the structure of slow and fast diffusing species on 0.01, 0.11 and 0.22 g/mL Soluplus solutions in water. The corresponding curves are shown as a function of the scattering vector q in Fig. 3, while the high concentration samples (0.11 and 0.22 g/mL) will be discussed in section 3.2.

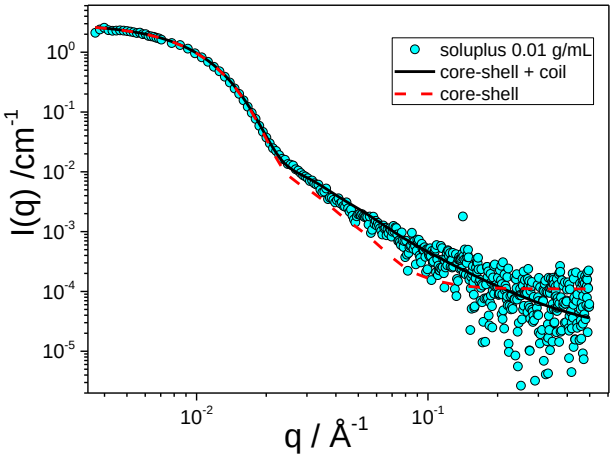

Figure 3. Azimuthal averaged SAXS curve as a function of the scattering vector q. Comparison of experimental data at 0.01 The core-shells model *plus* polymer coils (eqs.5-7) is reported as a solid line, while the dashed line is the model without the contribution of the polymer coil.

At the lowest concentration (0.01 g/mL), the contribution of the structure factor is not evident (S(q)~1) and the SAXS curve at low q-values is accounted for the form factor of core-shell spheres, while at high q-values the SAXS curve is consistent with the scattering expected by excluded volume of polymeric chains.

Accordingly, the overall SAXS curve has been fitted to a model where the polymer chains are subjected to excluded volume effects with a form factor, $P_{exV}(q)$, that coexist with spherical particles, modelled here as polydisperse core-shell structures having form factor <P(q)>, and structure factor S(q)=1. This fitting gives the overall dependence of the SAXS intensity on q described below:

$$I(q) = \phi_m(S(q)\langle P(q)\rangle) + \phi_{exV}\big(P_{exV}(q)\big) \qquad (5)$$

where ϕ_m is the micellar volume fraction and $\phi_{exV} = 1 - \phi_m$ is the free polymer volume fraction, which have been fixed on the basis on the dNMR results discussed above. The polydispersity was taken into account through the Schulz distribution of the core radius, R_c, and of the shell thickness, δ. The Schulz distributions is

also applied for the polydispersity of the effective radius, R_{eff}, that enters in the S(q) at high Soluplus concentrations.

The form factor of the polymer follows equation (6) below, given by Hammouda: [41]

$$P_{exV}(q) = \frac{1}{\nu(U)^{1/2\nu}} \int_0^U dt\ exp(-t)t^{\left(\frac{1}{2\nu}-1\right)} - \frac{1}{\nu(U)^{1/\nu}} \int_0^U dt\ exp(-t)t^{\left(\frac{1}{\nu}-1\right)} \quad (6)$$

Where ν is the excluded volume parameter equal to $1/m$, and m is the Porod exponent. U is $U = q^2 R_{g,coil}^2 (2\nu+1)(2\nu+2)/6$, where $R_{g,coil}$ is the radius of gyration of the polymer coil.

On the other hand, the form factor P(q) adopted for core-shell spherical particles is: [42]

$$P(q) = \frac{1}{V_s}\left[3V_c(\rho_c - \rho_{ps})\frac{sin(qR_c) - qR_c cos(qR_c)}{(qR_c)^3} + 3V_s(\rho_{ps} - \rho_s)\frac{sin\big(q(R_c+\delta_s)\big) - q(R_c+\delta_s)cos\big(q(R_c+\delta_s)\big)}{\big(q(R_c+\delta_s)\big)^3}\right]^2 + bkg \quad (7)$$

where V_s is the volume of the whole particle (=$(4\pi/3)(R_c+\delta_s)^3$), V_c is the core volume (=$(4\pi/3)(R_c)^3$, R_c is the core radius, δ_s is the thickness of the shell, ρ_c is the scattering length density of the core (in our case 10.5 10^{-6} Å^{-2}), ρ_{ps} is the scattering length density of the shell (9.56 10^{-6} Å^{-2}), while ρ_s is the scattering length density of the solvent water (9.46 x 10^{-6} Å^{-2}) and bkg refers to a factor that accounts for the background signal.

To avoid over-parametrization, ϕ_m was fixed to the fraction of slow phase detected by dNMR (P_{slow} in Table 1) and $\phi_{exV} = 1 - P_{slow}$ was the fixed fraction of free-polymer chain.

The resulting fit is shown in Fig. 3 and accounts for the experimental SAXS curve; best-fit parameters are listed in Table 2. For comparison, Fig. 3 also shows the best fit in the case of core-shell spheres without the presence of free coils. It is evident that spherical core-shell micelles can account only for the low q region (q< 0.02 Å^{-1}) and the presence of a 68% of polymer in form of (excluded volume) coil is required to describe the whole SAXS curve. This is a direct, independent, confirmation of the outcome of dNMR analysis discussed above.

Table 2 best-fit parameters obtained by fitting SAXS curves to eq. 5-7

Parameters	0.01 g/mL	0.10 g/mL	0.20 g/mL
R_c (nm)	16	16	16
Polydispersity (R_c)	0.2	0.3	0.3
δ_s (nm)	10	9	10
Polydispersity (δ_s)	0.2	0.25	0.3
R_{eff} (nm)	-	25	23.6
Polydispersity (R_{eff})	-	0.3	0.2
ϕ_p	-	0.28	0.43
$R_{g,coil}$ (nm)	5.5	5.5	5.5
Porod exp, m	2	2	1.7

Furthermore, the best fit parameters listed in Table 2 show that the radius of gyration of the coil ($R_{g,coil}$ = 5.5 nm) has a size that is close to the hydrodynamic radius associated to the fast diffusing species probed by

dNMR (r_h = 3 nm). For a homopolymer the ratio $R_{g,coil}/r_h$ is expected to be 1.5 for a Gaussian coil and larger in a good solvent [43] but, being Soluplus a grafted copolymer, a direct comparison with theories is precluded.

Considering the parameters of the core-shell spheres (i.e. core 16 nm plus shell 10 nm), the overall gyration radius equals the hydrodynamic radius obtained by dNMR (26 nm). For homogeneous spheres $R_{g,coil}/r_h$ =0.77, but here the core-shell particle is not homogeneous so we consider these results as a substantial agreement between SAXS and dNMR.

3.1.2 SLS

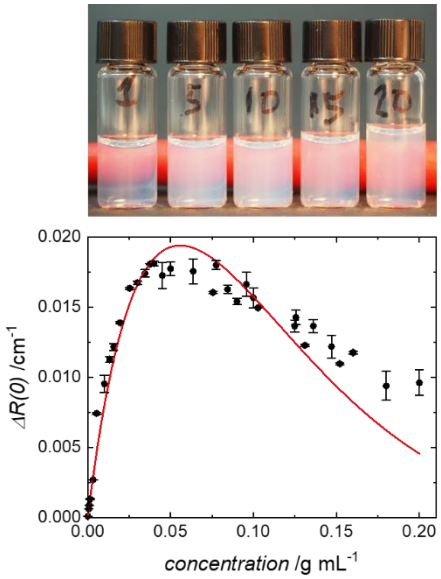

Figure 4. Up) Optical appearance of Soluplus aqueous solutions at 0.01, 0.05, 0.1, 0.15 and 0.20 g/mL from left to right. Down) Concentration dependence of the experimental excess Rayleigh ratios (black dots). The red solid line shows the theoretical intensity profile of hard spheres as calculated from the equation of Carnahan and Starling (eq.9).

The optical appearance of Soluplus solutions depends on the concentration in a peculiar way as shown in Fig. 4. Dilute and high concentrated solutions are slightly transparent but become highly opalescent at intermediate concentrations. Such a feature, detected by naked eye, can be quantitatively monitored *via* the average intensity of light scattered by the solution, and can be correlated to the osmotic compressibility. To do this, the data have been converted in absolute scattering intensities, i.e. "excess Rayleigh ratios, $\Delta\Re$, " as described in the experimental section. Strictly, the osmotic compressibility, i.e. the derivative of the osmotic pressure with the concentration, is correlated with the excess Rayleigh ratio measured at null scattering angle ($\Delta\Re(\theta=0)$). However, the small particle size, much smaller than the laser wavelength (663 nm), allows to avoid any extrapolation (i.e. $\Delta\Re(\theta)\sim\Delta\Re(0)$). The concentration-dependence of the experimental excess Rayleigh ratio is reported in Fig. 4 and confirms the existence of a maximum in the scattered light around 0.05 g/mL. Soluplus is a nonionic polymer and Laser Doppler Electrophoresis experiment (not shown) have found a null zeta-potential at all concentrations. Thus, it is interesting to compare the experimental data in Fig. 4 with the prediction for hard-spheres (HS) for which a maximum in scattered radiation is expected at a volume fraction (ϕ) around 0.1. Starting from the HS equation of state derived by Carnahan & Starling [44] it is possible to obtain the following relation for the for osmotic compressibility $\left(\frac{\partial\Pi}{\partial\phi}\right)$ written in terms of the HS volume fraction, ϕ:[45]

$$\frac{\partial\Pi}{\partial\phi} = \frac{k_bT}{\frac{4}{3}\pi R^3}\frac{(1+2\phi)^2-\phi^3(4-\phi)}{(1-\phi)^4} \qquad (8)$$

the volume fraction, ϕ, is related to the HS radius R by $\phi = \frac{N}{V}\cdot\frac{4}{3}\pi R^3$, where N is HS number and V the solution volume.

Accordingly, the excess Rayleigh ratio is

$$\Delta\Re(0) = K_{opt}\frac{k_bT\phi}{\frac{\partial\Pi}{\partial\phi}} = K_{opt}\frac{4}{3}\pi R^3\frac{\phi(1-\phi)^4}{(1+2\phi)^2-\phi^3(4-\phi)} \qquad (9)$$

To compare the experimental data with the prediction of eq. 9 we have to evaluate the HS volume fraction ϕ of the swollen polymer (including bound water) in terms of the polymer weight concentration C as:

$$\phi = \frac{v_{pol}+v_{W,bound}}{V} = \frac{v_{pol}}{V}(1+rv) = (1+rv)\frac{C}{\rho} \qquad (10)$$

Where v_{pol} and $v_{W,bound}$ are the volume of dry polymer and of bound water, respectively; $rv = v_{W,bound}/v_{pol}$ is the volume ratio between hydration water and polymer and ρ is the dry polymer density (g/mL).

A further complication arises because, as detailed in the previous section, there is evidence that only a fraction α of the total polymer is involved in the formation of the aggregates probed by light scattering experiments. This leads to:

$$\phi = H\alpha C \qquad (11)$$

Where $H = \frac{1+rv}{\rho}$ in mL/g is the specific volume of the swollen polymeric coil evaluated only with respect to the dry polymer weight, i.e. H is volume of (polymer + water) associated, in solution, to 1 g of micellized polymer (note that for Soluplus ρ~1 g/mL).

By exploiting eq. 11 the experimental data can be fitted to equation 9. αH is an adjustable parameter where H accounts for the contribution of hydration water in the aggregate's volume and α accounts for the possibility that a fraction of the polymer concentration is not involved in the micelle formation. The agreement between the resulting fit (shown in Fig. 4) and the experimental data is reasonable considering that equation 9 does not take into account any size polydispersity ; the best-fit value is αH= 2.33±0.05 mL/g.

As a whole, the results in Fig. 4 indicate that the HS model well describes the interactions among Soluplus aggregates, and this permits an estimate of their molar weight (Mw).

To do this, the excess Rayleigh ratio must be rewritten in terms of the weight concentration C as:

$$\Delta R(0) = K_{opt}\frac{RTC}{\frac{\partial\Pi}{\partial C}} = K_{opt}\frac{RTC}{\frac{\partial\Pi\partial\phi}{\partial\phi\partial C}} = K_{opt}C\alpha N_a\frac{\frac{4}{3}\pi R^3}{\alpha H}\frac{\phi(1-\phi)^4}{(1+2\phi)^2-\phi^3(4-\phi)} \qquad (12)$$

That can be arranged as

$$\frac{\Delta R(0)}{K_{opt}C}\left(\frac{\phi(1-\phi)^4}{(1+2\phi)^2-\phi^3(4-\phi)}\right)^{-1} = M_w \qquad (13)$$

Where $N_a\frac{\frac{4}{3}\pi R^3}{H} = M_w$ is the molar weight (g/mol) of the dry micelle (N_a is the Avogadro's number).

At low concentrations (C< 0.1 g/mL) the Mw oscillates around (6±1)x10^6 g/mol. Assuming the Soluplus molecular weight is 1.18 x10^5 g/mol [34], implies aggregates formed by ~ 50 polymer chains.

The data coming from the analysis of static light scattering intensity can be compared with the results obtained by dNMR and SAXS. Combining eqs. 12 and 13 under the assumption that HS have a radius $R \sim r_h \sim R_g =$ 26 nm, the following relationship is obtained:

$$\bar{V}_{mic} = N_a \frac{4}{3}\pi {r_h}^3 = M_w H \qquad (14)$$

This equation describes the relation between the radius coming from dNMR and SAXS with the M_w coming from independent static light scattering experiments. Where $\bar{V}_{mic}$ is the volume occupied by a mole of micelles that, for a radius of 26 nm, corresponds to 4.4 x10^7 mL/mol. Accordingly, $H = \frac{\bar{V}_{mic}}{M_w} = 7 \pm 1$ mL/g. This value combined with $\alpha H = 2.33 \pm 0.05$ mL/g from the best fit of the $\Delta\Re(0)$ vs. C in Fig. 4 gives an estimated value of $\alpha = 0.33 \pm 0.05$ that is fully consistent with the fraction ($P_{slow} = 0.32$) of polymer diffusing with the micelles probed by dNMR. Such an agreement can be taken as a "*a posteriori*" confirmation of the validity of the anszat $\Delta\Re(0) = \Delta\Re(\theta)$.

3.2 Two-state distribution of Soluplus chains: high concentration

Increasing Soluplus concentration above 0.1 g/mL results in a dramatic growth (two orders of magnitude) in the solution's viscosity. Such a sudden increase in viscosity can be rationalized in terms of HS colloidal dispersions approaching the maximum packing volume fraction. This is shown in Fig. 5 where the viscosity is plotted versus the HS volume fraction evaluated according to eq. 11 as $\phi = 2.33 \cdot C$ (outcome of the previous section). For reference, Fig. 5 also shows the best fit to the equation below, commonly used to describe the viscosity (η) of model HS dispersions. [46]

$$\eta = \frac{\eta^\circ}{\left(1 - \frac{\phi}{\phi_{max}}\right)^2} \qquad (15)$$

Where η° is the solvent viscosity and the only adjustable parameter is the maximum packing volume fraction ϕ_{max}. In the case of the data shown in Fig. 5, the best-fit value $\phi_{max} = 0.51$ is reasonably close to the ideal glass transition at which viscosity diverges ($\phi_{max} = 0.58$).[46].

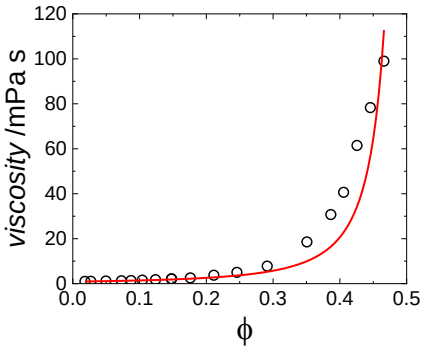

Figure 5. Experimental dependence of viscosity with the volume fraction evaluated for HS (empty dots) together with the best fit (red solid line) as calculated from the model HS dispersion (eq.15).

Despite the high viscosity, previous investigations report that for C < 0.2 g/mL, and at temperatures below 35 °C, Soluplus solutions still behave as Newtonian "viscous liquid material".[47] . Such a piece of information suggests that an evolution toward wormlike micelles is unlikely and concurs to ascribe the high viscosity to the jamming of the spherical aggregates. It is worth highlighting that shear thinning is often reported in polymer melts and solutions. The shear thinning in polymer solutions is usually attributed to the

disentanglement of polymer chains along the direction of the shear flow. [48,49]. However, this effect can only result in higher volume fractions.

The structure of the system in the high concentration range has been further investigated by dNMR and SAXS.

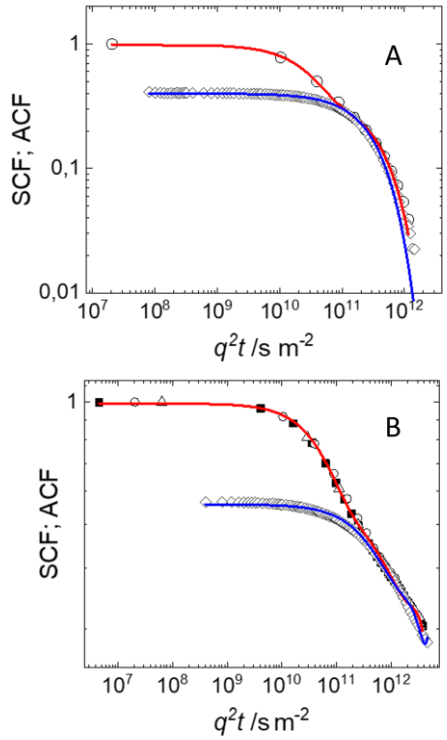

Figure 6. Comparison of the SCF (empty symbols and black squares) and ACF (empty diamonds) obtained with dNMR and DLS respectively for 0.11 (A) and 0.22 g/mL (B) Soluplus solutions. The corresponding diffusivities obtained from the fittings are presented in Table 1.

Fig. 6A shows the dNMR SCF of the Soluplus signal in solution at 0.109 g/mL (in D_2O). At such high concentration, a large part of the decay is dominated by a fast-diffusing component. Accordingly, the decay has been fitted to equation 3. 64% of the polymer is fast diffusing (D_{fast}~$3\cdot10^{-11}$ m^2/s) while 36% of the polymer has a diffusion coefficient that is one order of magnitude lower. Fig. 6A also shows the ACF measured with DLS on the very same sample and normalized to the contribution of the slow phase (P_{slow}) observed in the dNMR SCF. Inspection of Fig. 6A reveals how the DLS ACF superimposes to the slow phase of the dNMR SCF, confirming that also at this concentration DLS essentially probes the Brownian motion of the Soluplus large aggregates.

Increasing the concentration to 0.228 g/mL (the highest concentration explored) results in the SCF dNMR shown in Fig. 6B. In this case the SCF decay extends over a wide range of reciprocal diffusivities (q^2t) and it is still biphasic but the slow-diffusing component cannot be accounted for by a definite exponential decay. Instead, it appears to be “stretched”. To accurately probe such a decay, dNMR experiments performed using different Δ and δ (defined in the experimental section) have been combined (different symbols in Fig. 6B) to form a unique self-correlation function. The ACF collected by DLS on the same sample reproduces accurately the features of the slow-diffusing part of the SCF dNMR (see Fig. 6B). The “stretching” of the autocorrelation functions indicates that Soluplus experiences a large range of diffusivities, and this forces us to tailor the analysis accordingly.

Strictly eqs. 1 and 2 hold for monodisperse particles. For polydisperse samples the ACF (SFC) are no longer a single exponential, but rather are the sum of exponential decays, each accounting for the D_m (D_s) of a population of particles.

A robust way to account for this is according to the so-called cumulant expansion [50] where the ACF (SFC) is described by the exponential of the series:

$$ACF\ or\ SCF = exp\left(-\langle D\rangle q^2\tau + \frac{\sigma^2}{2}(q^2\tau)^2 + \frac{b}{3!}\tau(q^2\tau)^3 \dots \right) \quad (16)$$

where $\langle D\rangle$ is the mean and σ^2 is the variance of the distribution function of the appropriate diffusion coefficient. Accordingly, the ACF of DLS has been fitted to the above equation while the SCF from dNMR has been accounted for by the sum of a fast-diffusing exponential decay (eq. 3) and the cumulant expansion (eq. 16) obtaining:

$$SCF = (1 - P_{slow})exp\left(-D_{fast}q^2\tau\right) + P_{slow}exp\left(-\langle D\rangle q^2\tau + \frac{\sigma^2}{2}(q^2\tau)^2 + \frac{b}{3!}\tau(q^2\tau)^3 \dots \right) \quad (17)$$

To obtain a good fit, for both the ACF-DLS and the slow phase SCF-dNMR, the cumulant expansion must be extended to the fourth order. With such an approach we obtain mutually close best-fit values for the mean diffusion coefficient (~8x10^{-13} m^2/s) and standard deviation (~6x10^{-13} m^2/s) describing ACF-DLS and SCF-dNMR (see Table 1).

The SAXS curves collected on samples at C = 0.1 g/mL and C = 0.2 g/mL are shown in Fig. 7. Visual inspection suggests that, besides the obvious scaling of the scattered intensity due to the different concentration, the main features of the form factor observed at low concentration (0.01 g/mL in Fig. 3) are preserved at high concentration. For q-values > 0.02 Å^{-1} the trend, previously ascribed to core-shell spheres plus free polymer coils is preserved also at high concentration. At low-q it is evident that the effect of the structure factor, S(q) results in a peak in the overall SAXS curve. According to the nonionic nature of Soluplus and to the results of section 3.1.2 above, we have used the hard-sphere structure factor [51] for the interparticle structure factor, S(q), in equation 5 obtaining the effective radius, R_{eff}, and the the real hard spheres volume fraction ϕ_p. The repulsive interactions provide additional evidence that the micelles are stable even at high concentrations.

The best-fit parameters listed in Table 2 reveal that the core and shell dimensions of the particles are constant and equal to those determined for dilute solutions. The same holds for the gyration radius of the free polymer coil. The main effect of the increase in concentration is, thus, an increase in the particles volume fraction, ϕ_p. It is worth emphasising that the particle volume fraction obtained from the fitting of SAXS data (ϕ_p = 0.28 at C= 0.1 g/mL and ϕ_p = 0.43 at C= 0.2 g/mL) coincides with the assumption of hard sphere volume fraction (ϕ=2.33×C) found in the SLS analysis in the previous section.

According to SAXS results, Soluplus aggregates do not change in neither shape nor size, so the decrease of the diffusion coefficients in Table 1 with concentration must be associated to the hindrance of diffusion in a crowded environment.

3.3 Particle size and molecular weight close to the cmc.

The above reported data indicates the presence of large (26 nm) spherical core-shell aggregates in the range 0.01 g/mL – 0.2 g/mL coexisting with small ($R_{g,coil}$ = 5.5 nm) objects having the structure of polymeric coils. The amount of both forms is described by a predominance of the small species. It should be noticed that, although the relative fraction of small species slightly decreases with concentration, its net amount increases because the total polymer amount increases.

This scenario is somehow different from the one expected for classical micelle formation where, above the cmc, the unimer concentration remains steady and only the micelle concentration increases upon loading

the system. To make the situation more unusual, the cmc reported for Soluplus is extremely low. The manufacturer indicates a cmc of ~ $8x10^{-6}$ g/mL [19,34] but other studies indicate a much higher cmc-value ($8x10^{-4}$ g/mL [32], $5x10^{-4}$ g/mL [20]) that remains, however, well below the concentrations probed by dNMR and SAXS in the present work.

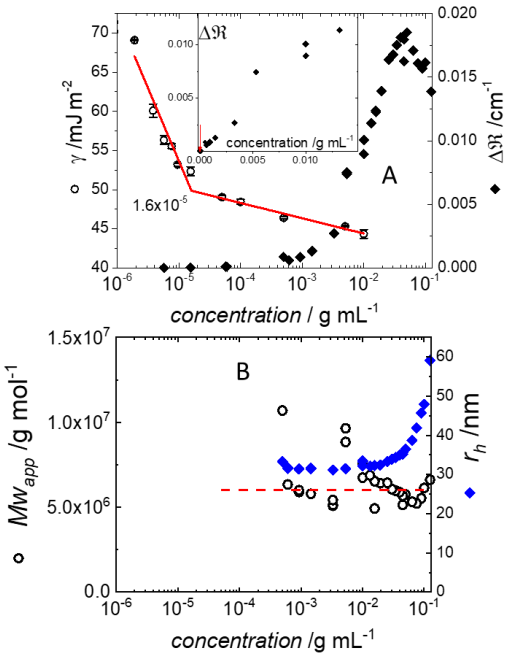

Figure 8. A) Experimental surface tension data (empty dots, left ordinate) and calculated excess Rayleigh ratios from SLS measurements (black diamonds, right ordinate) with increasing Soluplus concentration (log abscissa). In the inset the $\Delta\Re$ collected in the range C= $5x10^{-6}$ -0.013 g/mL are shown on a linear abscissa; the red arrow indicates the cmc.

B) Calculated apparent molecular weight (empty dots, left ordinate) and hydrodynamic radius obtained from DLS measurements (blue diamonds, right ordinate).

We have determined the cmc of our polymer batch by surface tension measurements and explored the very low concentration region close the cmc by DLS and SLS (the very low concentration range is not suitable for dNMR and SAXS investigations).

Surface tension measurements are shown in Fig. 8A. The surface tension decreases upon Soluplus loading and an evident break in the trend is observed at a concentration of $1.6x10^{-5}$ g/mL, a value that is very close to the cmc reported by the manufacturer (~ $8x10^{-6}$ g/mL). In the same graph (right ordinate) the excess Rayleigh ratios are reported, which represent an absolute measure of the intensity of scattered light. The light scattering is almost negligible for Soluplus concentrations below 10^{-3} g/mL but increases dramatically above that value, which is very close the Soluplus cmc reported in other research papers ($8x10^{-4}$ g/mL [32] and $5x10^{-4}$ g/mL [20].

The $\Delta\Re$ values have been transformed in molecular weight according to eq. 13 and their dependence on the concentration is shown in Fig. 8B together with the hydrodynamic radii obtained by DLS. For dilute solutions above the cmc, both the hydrodynamic size evaluated by DLS and the particle's molecular weight are independent from concentration. The size (r_h~30 nm) and molecular weight (~$6x10^6$ g/mol) are incompatible with the corresponding value of a Soluplus unimer (i.e. free chain). Therefore DLS and SLS measure aggregates that form at concentrations above 10^{-3} g/mL and increase in number upon further Soluplus loading (see the increase in $\Delta\Re$ values in Fig. 8A).

4. Discussion

The results of the previous section indicate that Soluplus spontaneously self-assembles into large spherical particles with a core-shell structure that remains constant up to the maximum concentration explored (0.2

g/mL). However, the critical concentration above which the formation of large objects takes place is 10^{-3} g/mL, which is more than two orders of magnitude above the cmc.

Furthermore, these aggregates represent only a fraction of Soluplus in solution, the large part of the polymer being arranged in form of small objects (r_h= 3 nm $R_{g,coil}$= 5.5 nm).

The concentration of large (C_L) and small (C_S) objects can be evaluated from the dNMR data in Table 1 as $C_L=P_{slow}*C$, and $C_S=(1-P_{slow})*C$, respectively.

Since the light scattered by the small object is negligible, the $\Delta\Re$ values in Figs. 4 and 8 are ascribable only to the large aggregates whose concentration can be evaluated as follows:

Eq. 9 can be rewritten as

$$\frac{\Delta\Re(0)}{K_{opt}\frac{4}{3}\pi R^3} = \frac{\phi(1-\phi)^4}{(1+2\phi)^2-\phi^3(4-\phi)} = f(\phi) \qquad (19)$$

Therefore, the experimental $\Delta\Re$ values allow the evaluation of the function *f(ϕ)*. The latter is a universal function of the HS volume fraction from which the value of ϕ can be numerically or graphically extracted.

Eventually, the concentration of large objects can be easily evaluated according to eq. 11 as $C_L = \alpha C = \frac{\phi}{H}$ and the concentration of small objects is C_S= C-C_L.

The evolution of the C_L and C_S, calculated from dNMR and SLS data, upon Soluplus loading is shown in Fig. 9.

There are two main pieces of information that can be extracted from Fig. 9. The first is that the data obtained through completely independent experiments and calculations agree. The only exception is the highest concentration probed by SLS (0.2 g/mL) but this is the condition where the fit of Fig. 4 poorly describes the data likely because the assumption of a constant amount of hydration water fails. The quantitative agreement between values coming from dNMR and SLS is a confirmation that the assumptions underlying the data analysis hold.

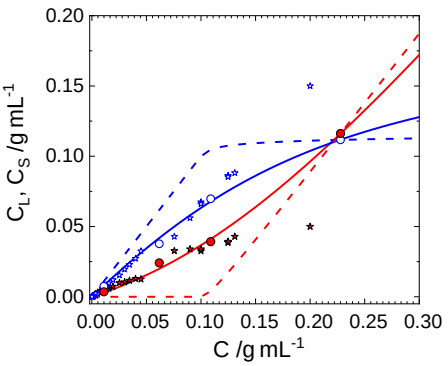

Figure 9. Variation in the concentrations of large (C_L, red symbols) and small (C_S, blue symbols) objects, calculated from dNMR (dots) and SLS (stars). The dashed lines, correspond to the theoretical concentrations of small (blue) and large (red) aggregates if the aggregation process would follow a traditional cooperative micellization process. The solid lines correspond to the theoretical calculations using a simplified model of a thermally activated isodesmic aggregation.

The second point is that we cannot simply consider the larger objects as conventional micelles and the smaller ones as unimers. Conventional micellization is a highly cooperative phenomenon in which the concentration of unimer in the micelles (C_{mic}) and in monomeric form (C_1) are correlated by the following relationship: [52]

$$C_{mic} = N[K_{mic}C_1]^N \qquad (20)$$

Where K_{mic} is the equilibrium constant for micelle formation and N is the aggregation number. Eq. 20 foretells that before the cmc~ $1/K_{mic}$ the C_{mic} is negligible so all added substance stays in solution as monomers. Above the cmc C_1 remains constant and equal to the cmc, and loading the system increases C_{mic}.

For reference, Fig. 8 shows the C_{mic} and C_1 evaluated according to eq. 20, assuming N=50. The dependence of the experimental data coming from independent techniques on the concentration is completely different from the prediction of the model.

The coexistence of large and small species suggests a lower level of cooperativity than that implicit in eq. 20. In addition, the presence of large aggregates starts at a concentration that is a hundred times larger than the cmc, suggesting that their formation does not involve Soluplus monomers (whose concentration should be constant at 10^{-5} g/ml).

Another possibility is that the large aggregates self-assemble starting from smaller ones that, therefore, should be identified as "primary" micelles. Such an aggregation must be non-cooperative (isodesmic) and, to justify the large values of C_s observed, it requires the activation of the small aggregates.

The minimal model is based on two steps:

An unfavourable activated process with equilibrium constant K_{att}<1

$$S \overset{K_{att}}{\leftrightarrows} S^*$$

in which the small particles (S) are thermally activated to produce the species (S*) that can undergo further self-assembly to form a large aggregate made of *n* small particles (n=2, 3, ..)

$$S^* + S^* \overset{K_{sa}}{\leftrightarrows} L_2$$

$$L_{n-1} + S^* \overset{K_{sa}}{\leftrightarrows} L_n$$

For the sake of simplicity, we suppose the equilibrium constants of these self-assembly reaction independent from index n and equal to $K_{sa} = \frac{[L_n]}{[S^*][L_{n-1}]} = \frac{[L_2]}{[S^*]^2}$ so that the concentration of large particles produced by the fusion of n primary small particles is $[L_n]=[S^*]^n K_{sa}^{n-1}$

The mass conservation requires the total concentration to be:

$$C = [S] + [S^*] + \sum_{n=2}^{m} n[L_n] = [S] + [S^*] + [S^*] \sum_{n=2}^{m} n([S^*]K_{sa})^{n-1} \quad (21)$$

The total concentration of small particles measured by dNMR or SLS is $C_S = [S]+[S^*]$. In terms of such experimentally accessible quantity the concentration of activated reactants is $[S^*] = C_S K_{att}/(1+K_{att}) = C_S A$ with A<1, so eq. 21 can be rewritten as:

$$C = C_s + C_s A \sum_{n=2}^{m} n(C_s A K_{sa})^{n-1} \quad (22)$$

Where m is the maximum generalized aggregation number. As long as the term $C_S AK_{sa}$ <1 and m is large enough, the sum in eq. 22 can be simplified using the expression for the sum of geometrical series to obtain:

$$C = C_s + C_s A \frac{2 - C_s A K_{sa}}{(1 - C_s A K_{sa})^2} \qquad (23)$$

The experimental values of C and C_s of Fig. 9 have been fitted to the above equation and the resulting fit is shown as a continuous blue line. Also shown are the results for C_L=C-C_s. Such a simplified model for thermal activated isodesmic aggregation successfully describes the experimental data. It is worth noting that previous isothermal calorimetry (ITC) investigations [20, 30] point to a non-conventional micellization behaviour of Soluplus. Indeed, the heat of dilution doesn't show the customary sigmoidal behaviour and has the largest change well above the cmc at the concentration (~10^{-3} g/mL) where we start to probe the presence of large aggregates. It thus conceivable that what ITC was probing is the isodesmic self-assembly of small micelles into largest aggregates.

In principle, the size of these small objects, as probed by SAXS and dNMR, could also be compatible with single Soluplus chains but their concentration is very high (they are the most abundant species in solution) which is incompatible with the low cmc value. Accordingly, we suppose the small objects are the primary micelles formed for C > 10^{-5} g/mL and that they are formed by few unimers that form dimers or trimers preserving a polymer coil conformation.

We note that eq. 23 can also be obtained assuming the activation step is associated to the formation of L_2 if the equilibrium constant is smaller than the subsequent growth steps (formation of L_m with m>2). Presently, the nature of the activation step is unknown. However, considering the compact nature of the large aggregates core and the loose coil conformation of the small species, one can speculate the activation step could be due to the drastic change in conformation required to pack many polymers coils into a large micelles.

5. Conclusion

In this contribution we have combined several experimental techniques (dNMR, SAXS, SLS, DLS, viscosity and surface tension measurements) to study the microstructure of Soluplus solutions in a wide range of concentration reminiscent the final part of the oral route of administration of this polymer.

We found that in solution, even at high loading, Soluplus is present as two species differing in size by one order of magnitude. This has not been recognized in previous investigations that have only reported the presence of micelles (r_h= 35 nm) observed at room T by DLS and TEM. [17,24,39]. The reason is that these techniques are biased toward large particles and, in the case of coexistence, fail to detect small objects. The overall picture of this "large micelles" is that of spherical core-shell particles made by ~ 50 unimers, strongly hydrated (6 ml of water per g of dry polymer) and interacting essentially as HS. However, only a minor fraction of the Soluplus is present in this form. Large part of the polymer (60%-50% depending on the concentration) is present as smaller species with a structure that is analogous to a (excluded-volume) polymeric coil forming above the cmc (10^{-5} g/mL) and growing in number upon polymer loading until (for C > 10^{-3} g/mL) they self-assembly to form micelles leading to coexistence between polymer coil and micellar structures. Interestingly, the formation of "large micelles" from "small micelles" is a non-cooperative isodesmic process triggered by an activation step.

The presence of weakly cooperative aggregation has been previously reported for grafted hydrophobically modified polyelectrolytes.[53,54] In particular, NMR and fluorescence investigations of hydrophobically modified polyacrylates (HMPAs), indicated that free unimers coexist with large aggregates, and that their concentration increases above the cmc (in this sense, the data in Figure 5 of ref. [53]are very similar to the data shown here in Figure 9), but such a aggregation was not explicitly modelled. In the case of the HMPAs,

the low cooperativity was ascribed to the dispersion in grafting density, which could also play a role in the present case.

It should be stressed that, in the case of HMPAs, the weakly cooperative association involves unimers that self-assemble into aggregates while, in the case of Soluplus, the isodesmic aggregation involves small primary micelles that self-assemble into larger aggregates. This evidence suggests the role of drug adsorption enhancer played by Soluplus [21,55] could be associated also to these smaller micelles that have been unnoticed in previous investigations. Furthermore, the presence of a thermally activated step is intriguing considering that Soluplus is known to have a lower critical solution temperature around 35 °C.

In the future, a more thorough understanding of the relationship between the Soluplus microstructure and its role as enhancer of drug adsorption will require the extension of this multi-technique characterization at physiological temperatures and pH-values.

Declaration of Competing Interest

The authors declare that they have no known competing financial interests or personal relationships that could have appeared to influence the work reported in this paper.

Acknowledgements

CSGI (Consorzio Interuniversitario per lo Sviluppo dei Sistemi a Grande Interfase) project Nuovi Materiali Funzionali CMPT191138, POR PUGLIA FESR-FSE 2014/2020 Research for Innovation (REFIN)-Codice Pratica: 7BDC8679 are acknowledged for financial support. The Authors are grateful to Prof. Emiliano Fratini for fruitful discussion.

[1] G. Tsakiridou, C. Reppas, M. Kuentz, L. Kalantzi, A novel rheological method to assess drug-polymer interactions regarding miscibility and crystallization of drug in amorphous solid dispersions for oral drug delivery, Pharmaceutics. 11 (2019). https://doi.org/10.3390/pharmaceutics11120625.

[2] E. Guzmán, A. Mateos-Maroto, M. Ruano, F. Ortega, R.G. Rubio, Layer-by-Layer polyelectrolyte assemblies for encapsulation and release of active compounds, Adv. Colloid Interface Sci. 249 (2017) 290–307. https://doi.org/10.1016/J.CIS.2017.04.009.

[3] M. Ghezzi, S. Pescina, C. Padula, P. Santi, E. Del Favero, L. Cantù, S. Nicoli, Polymeric micelles in drug delivery: An insight of the techniques for their characterization and assessment in biorelevant conditions, J. Control. Release. 332 (2021) 312–336. https://doi.org/10.1016/j.jconrel.2021.02.031.

[4] J.K. Patra, G. Das, L.F. Fraceto, E.V.R. Campos, M. del P. Rodriguez-Torres, L.S. Acosta-Torres, L.A. Diaz-Torres, R. Grillo, M.K. Swamy, S. Sharma, S. Habtemariam, H.-S. Shin, Nano based drug delivery systems: recent developments and future prospects, J. Nanobiotechnology 2018 161. 16 (2018) 1–33. https://doi.org/10.1186/S12951-018-0392-8.

[5] W. Xu, P. Ling, T. Zhang, Polymeric Micelles, a Promising Drug Delivery System to Enhance Bioavailability of Poorly Water-Soluble Drugs, J. Drug Deliv. 2013 (2013) 1–15.

https://doi.org/10.1155/2013/340315.

[6] A.R. Nair, Y.D. Lakshman, V. Sai, K. Anand, K.S.N. Sree, K. Bhat, S.J. Dengale, Overview of Extensively Employed Polymeric Carriers in Solid Dispersion Technology, AAPS PharmSciTech. 21 (2020) 309. https://doi.org/10.1208/s12249-020-01849-z.

[7] polymeric micelles (All Fields) – 5,746 – Web of Science Core Collection, (n.d.). https://www.webofscience.com/wos/woscc/summary/58273861-d52c-43c3-af5a-6c2733c352fd-0306af37/relevance/1 (accessed August 3, 2021).

[8] Y. Lu, E. Zhang, J. Yang, Z. Cao, Strategies to improve micelle stability for drug delivery, (n.d.). https://doi.org/10.1007/s12274-018-2152-3.

[9] A. Vonarbourg, C. Passirani, P. Saulnier, J.P. Benoit, Parameters influencing the stealthiness of colloidal drug delivery systems, Biomaterials. 27 (2006) 4356–4373. https://doi.org/10.1016/j.biomaterials.2006.03.039.

[10] D.E. Owens, N.A. Peppas, Opsonization, biodistribution, and pharmacokinetics of polymeric nanoparticles, Int. J. Pharm. 307 (2006) 93–102. https://doi.org/10.1016/J.IJPHARM.2005.10.010.

[11] F. Alexis, E. Pridgen, L.K. Molnar, O.C. Farokhzad, Factors Affecting the Clearance and Biodistribution of Polymeric Nanoparticles, Mol. Pharm. 5 (2008) 505–515. https://doi.org/10.1021/MP800051M.

[12] M.E. Fox, F.C. Szoka, J.M.J. Fréchet, Soluble Polymer Carriers for the Treatment of Cancer: The Importance of Molecular Architecture, Acc. Chem. Res. 42 (2009) 1141–1151. https://doi.org/10.1021/AR900035F.

[13] R.K. Jain, Transport of molecules across tumor vasculature, Cancer Metastasis Rev. 1987 64. 6 (1987) 559–593. https://doi.org/10.1007/BF00047468.

[14] E. Blanco, H. Shen, M. Ferrari, Principles of nanoparticle design for overcoming biological barriers to drug delivery, Nat. Biotechnol. 33 (2015) 941–951. https://doi.org/10.1038/nbt.3330.

[15] Y. Liu, W. Wang, J. Yang, C. Zhou, J. Sun, pH-sensitive polymeric micelles triggered drug release for extracellular and intracellular drug targeting delivery, Asian J. Pharm. Sci. 8 (2013) 159–167. https://doi.org/10.1016/J.AJPS.2013.07.021.

[16] M. Linn, E.M. Collnot, D. Djuric, K. Hempel, E. Fabian, K. Kolter, C.M. Lehr, Soluplus® as an effective absorption enhancer of poorly soluble drugs in vitro and in vivo, Eur. J. Pharm. Sci. 45 (2012) 336–343. https://doi.org/10.1016/j.ejps.2011.11.025.

[17] D. Xia, H. Yu, J. Tao, J. Zeng, Q. Zhu, C. Zhu, Y. Gan, Supersaturated polymeric micelles for oral cyclosporine A delivery: The role of Soluplus-sodium dodecyl sulfate complex, Colloids Surfaces B Biointerfaces. 141 (2016) 301–310. https://doi.org/10.1016/j.colsurfb.2016.01.047.

[18] Y. Zeng, S. Li, C. Liu, T. Gong, X. Sun, Y. Fu, Z. Zhang, Soluplus micelles for improving the oral bioavailability of scopoletin and their hypouricemic effect in vivo, Acta Pharmacol. Sin. 2017 383. 38 (2017) 424–433. https://doi.org/10.1038/aps.2016.126.

[19] G.V. Bonde, G. Ajmal, S.K. Yadav, P. Mittal, J. Singh, B. V. Bakde, B. Mishra, Assessing the viability of Soluplus® self-assembled nanocolloids for sustained delivery of highly hydrophobic lapatinib (anticancer agent): Optimisation and in-vitro characterisation, Colloids Surfaces B Biointerfaces. 185 (2020). https://doi.org/10.1016/j.colsurfb.2019.110611.

[20] J.F. Alopaeus, E. Hagesæther, I. Tho, Micellisation Mechanism and Behaviour of Soluplus®–Furosemide Micelles: Preformulation Studies of an Oral Nanocarrier-Based System, Pharm. 2019, Vol.

12, Page 15. 12 (2019) 15. https://doi.org/10.3390/PH12010015.

[21] R.N. Shamma, M. Basha, Soluplus®: A novel polymeric solubilizer for optimization of Carvedilol solid dispersions: Formulation design and effect of method of preparation, Powder Technol. 237 (2013) 406–414. https://doi.org/10.1016/j.powtec.2012.12.038.

[22] F. Alvarez-Rivera, D. Fernández-Villanueva, A. Concheiro, C. Alvarez-Lorenzo, α-Lipoic Acid in Soluplus® Polymeric Nanomicelles for Ocular Treatment of Diabetes-Associated Corneal Diseases, J. Pharm. Sci. 105 (2016) 2855–2863. https://doi.org/10.1016/j.xphs.2016.03.006.

[23] A. Varela-Garcia, A. Concheiro, C. Alvarez-Lorenzo, Soluplus micelles for acyclovir ocular delivery: Formulation and cornea and sclera permeability, Int. J. Pharm. 552 (2018) 39–47. https://doi.org/10.1016/J.IJPHARM.2018.09.053.

[24] I. Salah, M.A. Shamat, M.T. Cook, Soluplus solutions as thermothickening materials for topical drug delivery, J. Appl. Polym. Sci. 136 (2019) 46915. https://doi.org/10.1002/APP.46915.

[25] S.F. Taveira, A. Varela-Garcia, B. dos Santos Souza, R.N. Marreto, M. Martin-Pastor, A. Concheiro, C. Alvarez-Lorenzo, Cyclodextrin-based poly(pseudo)rotaxanes for transdermal delivery of carvedilol, Carbohydr. Polym. 200 (2018) 278–288. https://doi.org/10.1016/J.CARBPOL.2018.08.017.

[26] H. Wu, K. Wang, H. Wang, F. Chen, W. Huang, Y. Chen, J. Chen, J. Tao, X. Wen, S. Xiong, Novel self-assembled tacrolimus nanoparticles cross-linking thermosensitive hydrogels for local rheumatoid arthritis therapy, Colloids Surfaces B Biointerfaces. 149 (2017) 97–104. https://doi.org/10.1016/J.COLSURFB.2016.10.013.

[27] X. Jin, B. Zhou, L. Xue, W. San, Soluplus® micelles as a potential drug delivery system for reversal of resistant tumor, Biomed. Pharmacother. 69 (2015) 388–395. https://doi.org/10.1016/j.biopha.2014.12.028.

[28] M. Saydam, W.P. Cheng, N. Palmer, F. Mawas, R. Francis, K. MacLellan-Gibson, A. Khan, Nano-sized Soluplus® polymeric micelles enhance the induction of tetanus toxin neutralising antibody response following transcutaneous immunisation with tetanus toxoid, Vaccine. 35 (2017) 2489–2495. https://doi.org/10.1016/j.vaccine.2017.03.012.

[29] A. Melocchi, F. Parietti, A. Maroni, A. Foppoli, A. Gazzaniga, L. Zema, Hot-melt extruded filaments based on pharmaceutical grade polymers for 3D printing by fused deposition modeling, Int. J. Pharm. 509 (2016) 255–263. https://doi.org/10.1016/J.IJPHARM.2016.05.036.

[30] N.-Q. Shi, H.-W. Lai, Y. Zhang, B. Feng, X. Xiao, H.-M. Zhang, Z.-Q. Li, X.-R. Qi, On the inherent properties of Soluplus and its application in ibuprofen solid dispersions generated by microwave-quench cooling technology, Https://Doi.Org/10.1080/10837450.2016.1256409. 23 (2016) 573–586. https://doi.org/10.1080/10837450.2016.1256409.

[31] M.F. Simões, A. Pereira, S. Cardoso, S. Cadonau, K. Werner, R.M.A.A. Pinto, S. Simões, Five-Stage Approach for a Systematic Screening and Development of Etravirine Amorphous Solid Dispersions by Hot-Melt Extrusion, Mol. Pharm. 17 (2020) 554–568. https://doi.org/10.1021/acs.molpharmaceut.9b00996.

[32] S. Tanida, T. Kurokawa, H. Sato, K. Kadota, Y. Tozuka, Evaluation of the micellization mechanism of an amphipathic graft copolymer with enhanced solubility of ipriflavone, Chem. Pharm. Bull. 64 (2016) 68–72. https://doi.org/10.1248/cpb.c15-00655.

[33] Nikita., M. Aqil, Y. Sultana, A grafted copolymer-based nanomicelles for topical ocular delivery of everolimus: Formulation, characterization, ex-vivo permeation, in-vitro ocular toxicity, and stability study, Eur. J. Pharm. Sci. 159 (2021) 105735. https://doi.org/10.1016/J.EJPS.2021.105735.

[34] BASF, Technical Information Soluplus, BASF, Pharma Ingredients Serv. (2010) 1–8.

[35] U. Olsson, P. Schurtenberger, Structure, Interactions, and Diffusion in a Ternary Nonionic Microemulsion Near Emulsification Failure, Langmuir. 9 (1993) 3389–3394. https://doi.org/10.1021/la00036a011.

[36] C.S. Johnson, Diffusion ordered nuclear magnetic resonance spectroscopy: Principles and applications, Prog. Nucl. Magn. Reson. Spectrosc. 34 (1999) 203–256. https://doi.org/10.1016/S0079-6565(99)00003-5.

[37] G. Colafemmina, H. Mateos, G. Palazzo, Diffusion NMR studies of complex liquid formulations, Curr. Opin. Colloid Interface Sci. (2020). https://doi.org/10.1016/j.cocis.2020.04.006.

[38] G. Palazzo, L. Paduano, Diffusion measuring techniques (Chapter 10), in: D. Berti, G. Palazzo (Eds.), Colloid. Found. Nanosci., 2nd ed., Elsevier, 2021: pp. 199–231.

[39] J.M.O. Pinto, A.F.C. Rengifo, C. Mendes, A.F. Leão, A.L. Parize, H.K. Stulzer, Understanding the interaction between Soluplus® and biorelevant media components, Colloids Surfaces B Biointerfaces. 187 (2020) 110673. https://doi.org/10.1016/j.colsurfb.2019.110673.

[40] G. Palazzo, H. Mateos, D. Berti, Diffusion, aggregation and electrokinetics, Colloid. Found. Nanosci. (2022) 201–225. https://doi.org/10.1016/B978-0-12-822089-4.00006-4.

[41] B. Hammouda, SANS from homogeneous polymer mixtures: A unified overview, Adv. Polym. Sci. 106 (1993) 87–133. https://doi.org/10.1007/BFB0025862.

[42] A. Guinier, G. Fournet, C.B. Walker, G.H. Vineyard, Small-Angle Scattering of X-Rays, Phys. Today. 9 (2009) 38. https://doi.org/10.1063/1.3060069.

[43] B. Dünweg, D. Reith, M. Steinhauser, K. Kremer, Corrections to scaling in the hydrodynamic properties of dilute polymer solutions, J. Chem. Phys. 117 (2002) 914. https://doi.org/10.1063/1.1483296.

[44] N.F. Carnahan, K.E. Starling, Equation of State for Nonattracting Rigid Spheres, J. Chem. Phys. 51 (2003) 635. https://doi.org/10.1063/1.1672048.

[45] W. Brown, K. Schillén, M. Almgren, S. Hvidt, P. Bahadur, Micelle and Gel Formation In a Poly(ethylene oxide)/Poly(propylene oxide)/ Poly(ethylene oxide) Trlblock Copolymer in Water Solution. Dynamic and Static Light Scattering and Oscillatory Shear Measurements, 1991. https://pubs.acs.org/sharingguidelines (accessed March 1, 2020).

[46] J. Mewis, N.J. Wagner, Colloidal Suspension Rheology, Colloid. Suspens. Rheol. 9780521515993 (2011) 1–393. https://doi.org/10.1017/CBO9780511977978.

[47] M. Cespi, L. Casettari, G.F. Palmieri, D.R. Perinelli, G. Bonacucina, Rheological characterization of polyvinyl caprolactam–polyvinyl acetate–polyethylene glycol graft copolymer (Soluplus®) water dispersions, Colloid Polym. Sci. 2013 2921. 292 (2013) 235–241. https://doi.org/10.1007/S00396-013-3077-8.

[48] M.T. Shaw, Introduction to polymer rheology, (2012) 395.

[49] M. Youssry, F. Asaro, L. Coppola, L. Gentile, I. Nicotera, Solution microstructures of the micellar phase of Pluronic L64/SDS/water system, J. Colloid Interface Sci. 342 (2010) 348–353. https://doi.org/10.1016/J.JCIS.2009.10.069.

[50] D.E. Koppel, Analysis of Macromolecular Polydispersity in Intensity Correlation Spectroscopy: The Method of Cumulants, J. Chem. Phys. 57 (1972) 4814. https://doi.org/10.1063/1.1678153.

[51] J.K. Percus, G.J. Yevick, Analysis of Classical Statistical Mechanics by Means of Collective Coordinates, Phys. Rev. 110 (1958) 1. https://doi.org/10.1103/PhysRev.110.1.

[52] J.N. Israelachvili, Intermolecular and Surface Forces, Elsevier, 2011. https://doi.org/10.1016/B978-0-12-375182-9.10019-3.

[53] F. Petit-Agnely, I. Iliopoulos, Aggregation mechanism of amphiphilic associating polymers studied by 19F and 13C nuclear magnetic resonance, J. Phys. Chem. B. 103 (1999) 4803–4808. https://doi.org/10.1021/jp984830z.

[54] I. Furó, I. Iliopoulos, P. Stilbs, Structure and Dynamics of Associative Water-Soluble Polymer Aggregates As Seen by 19F NMR Spectroscopy, J. Phys. Chem. B. 104 (2000) 485–494. https://doi.org/10.1021/jp9927404.

[55] K. Kolter, M. Karl, A. Gryczke, B. Se, Hot-Melt Extrusion with BASF Pharma Polymers Extrusion Compendium 2nd Revised and Enlarged Edition, (2012).

5: Figure 1

Click here to access/download;5: Figure;fig1.tif

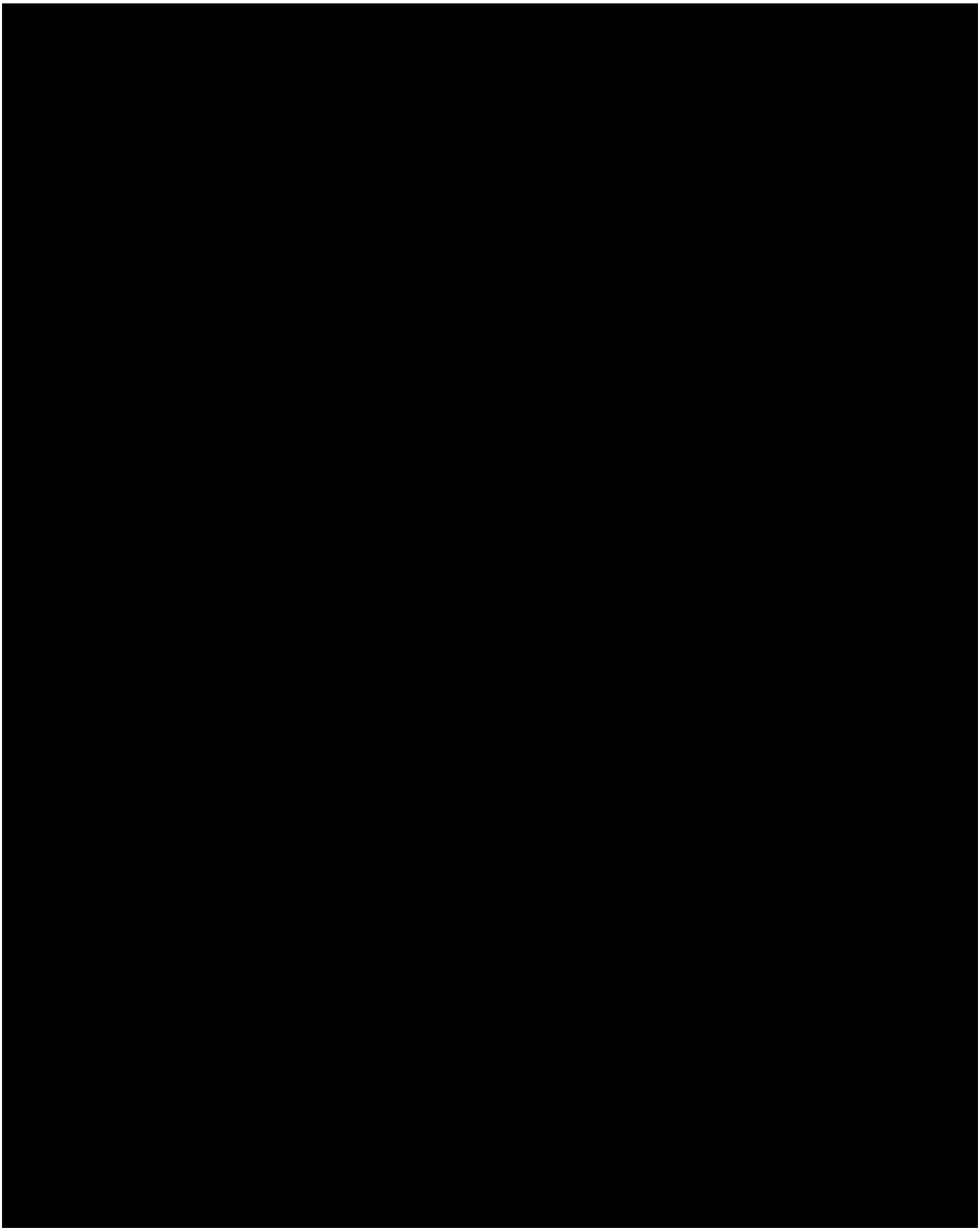

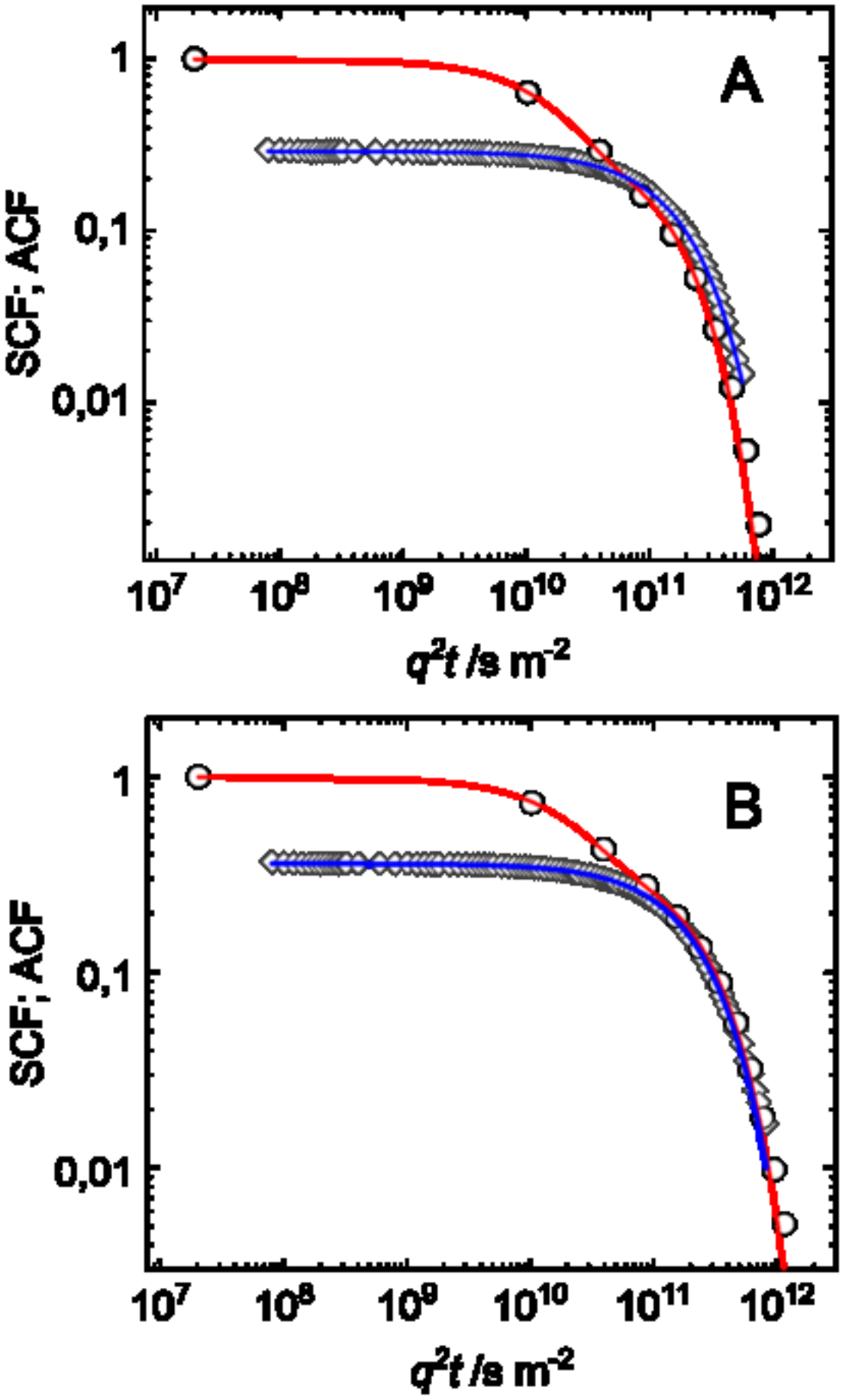

5: Figure 3

Click here to access/download;5: Figure;fig3.tif

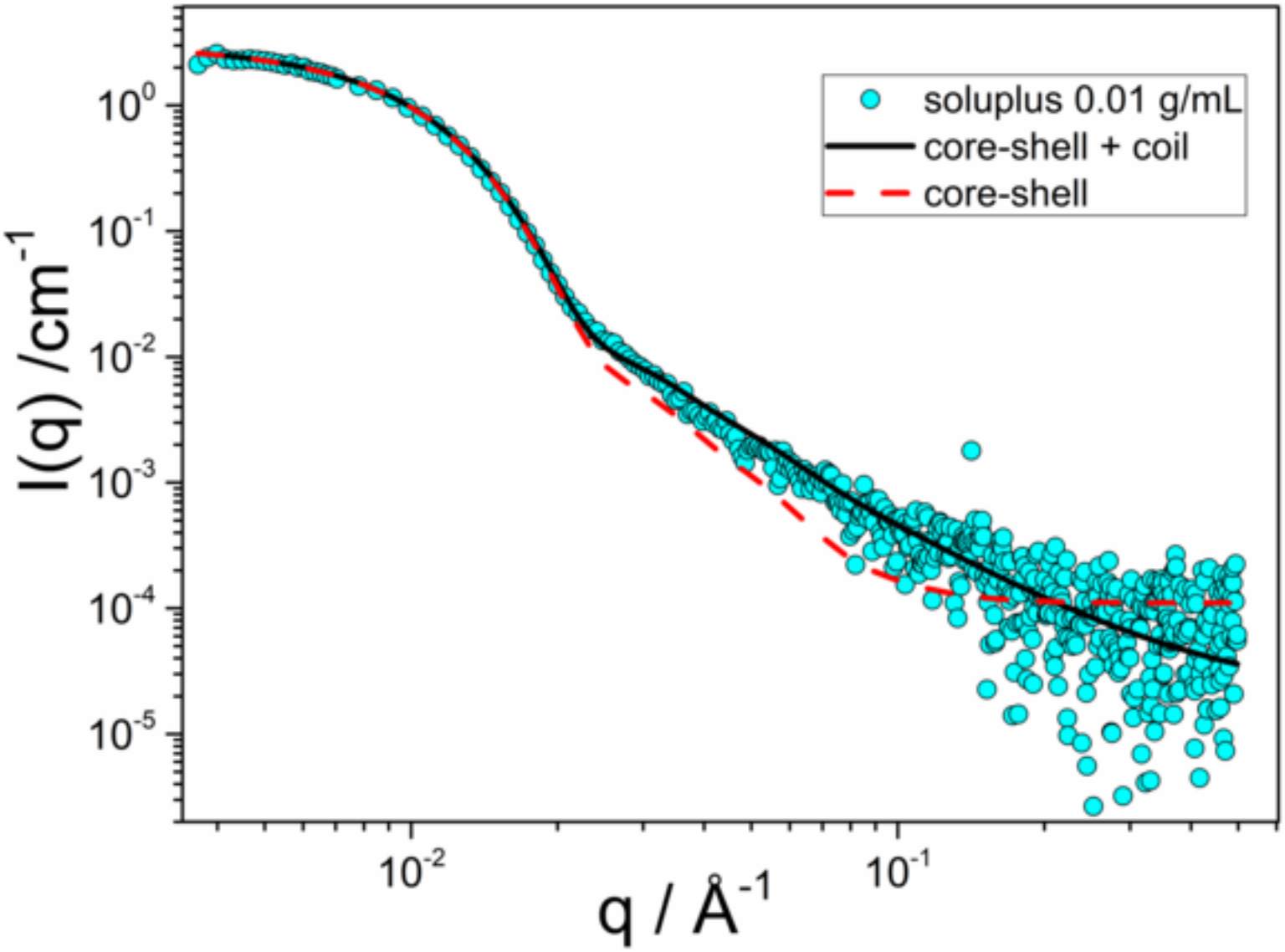

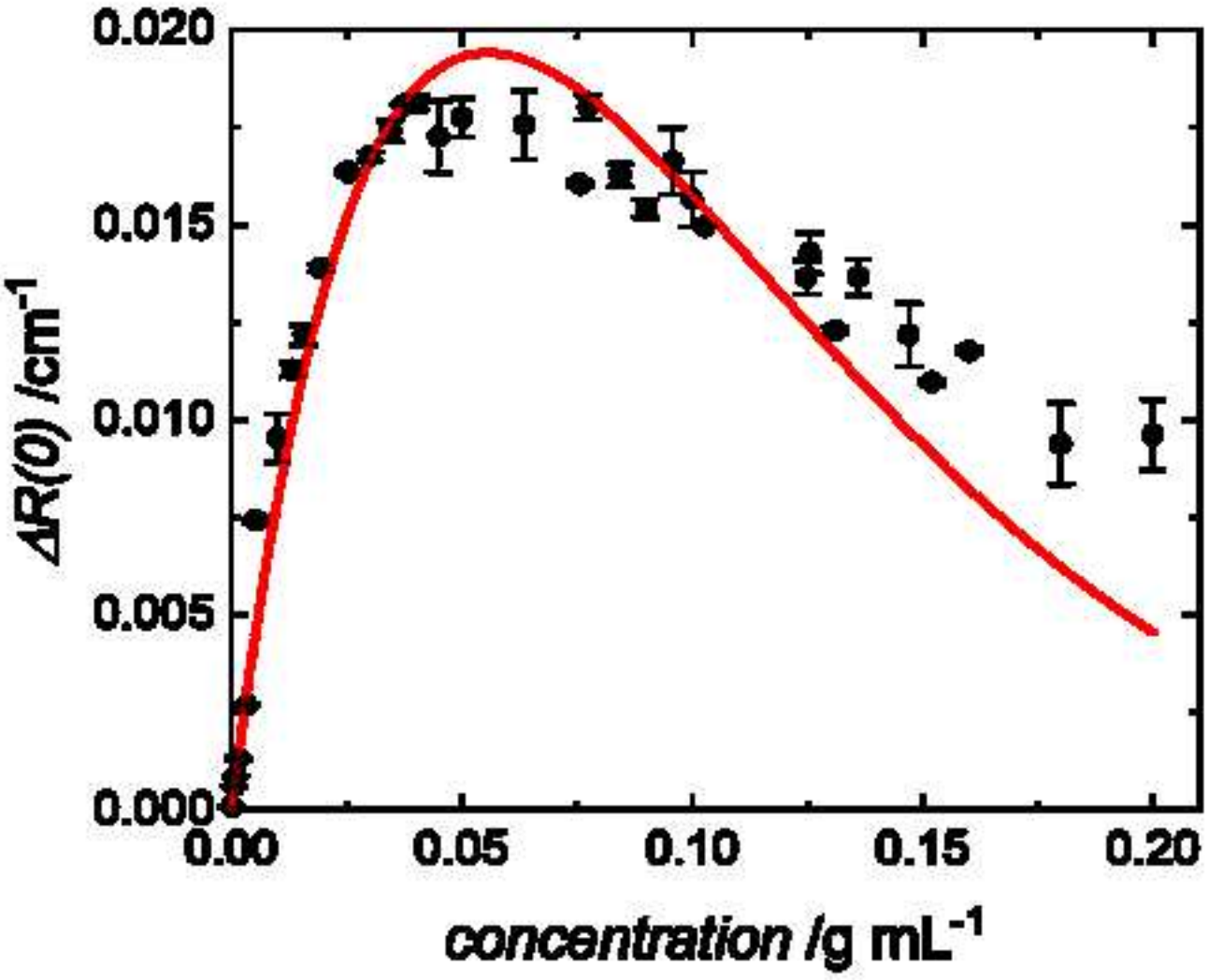

5: Figure 5

Click here to access/download;5: Figure;fig5.tif

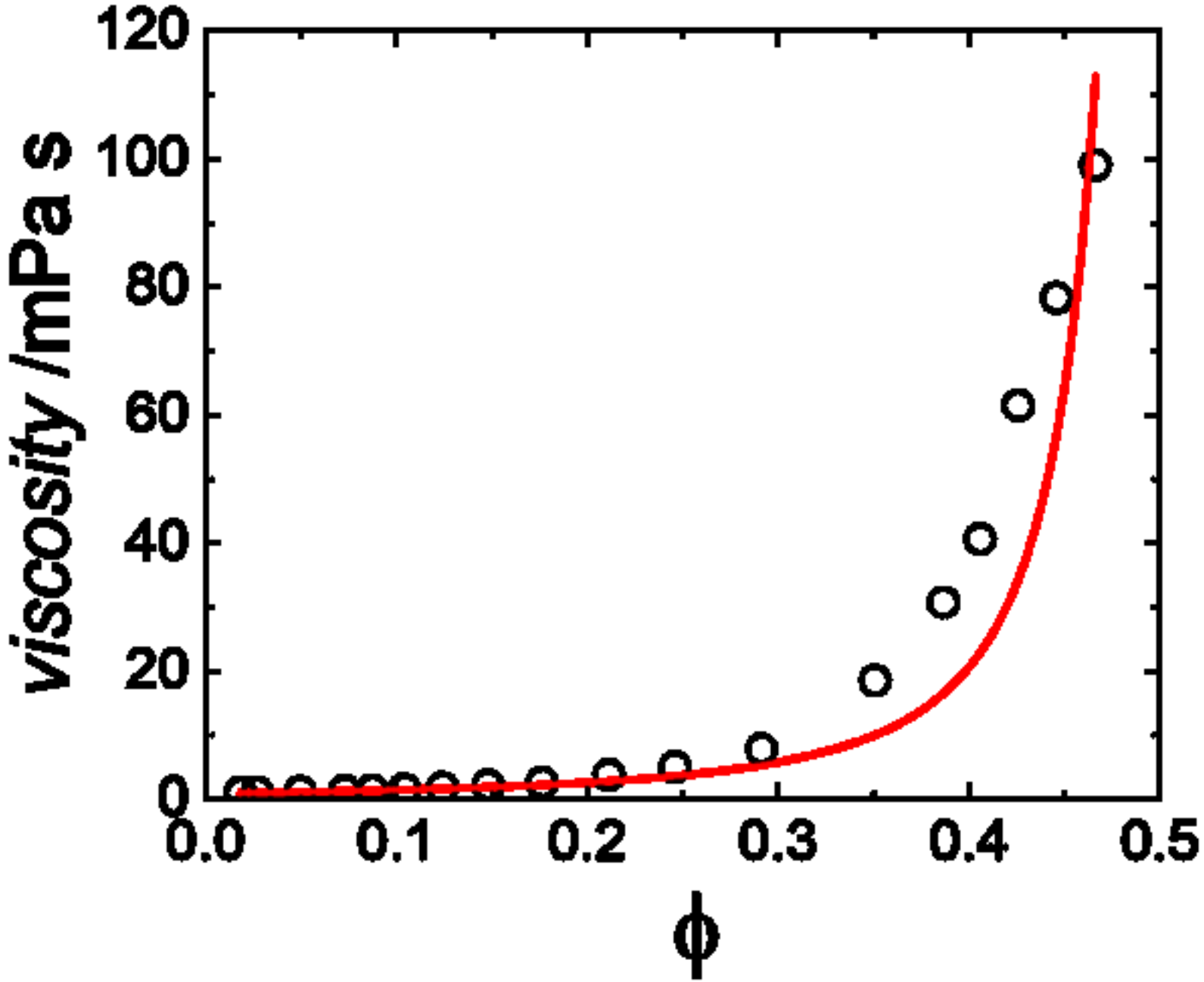

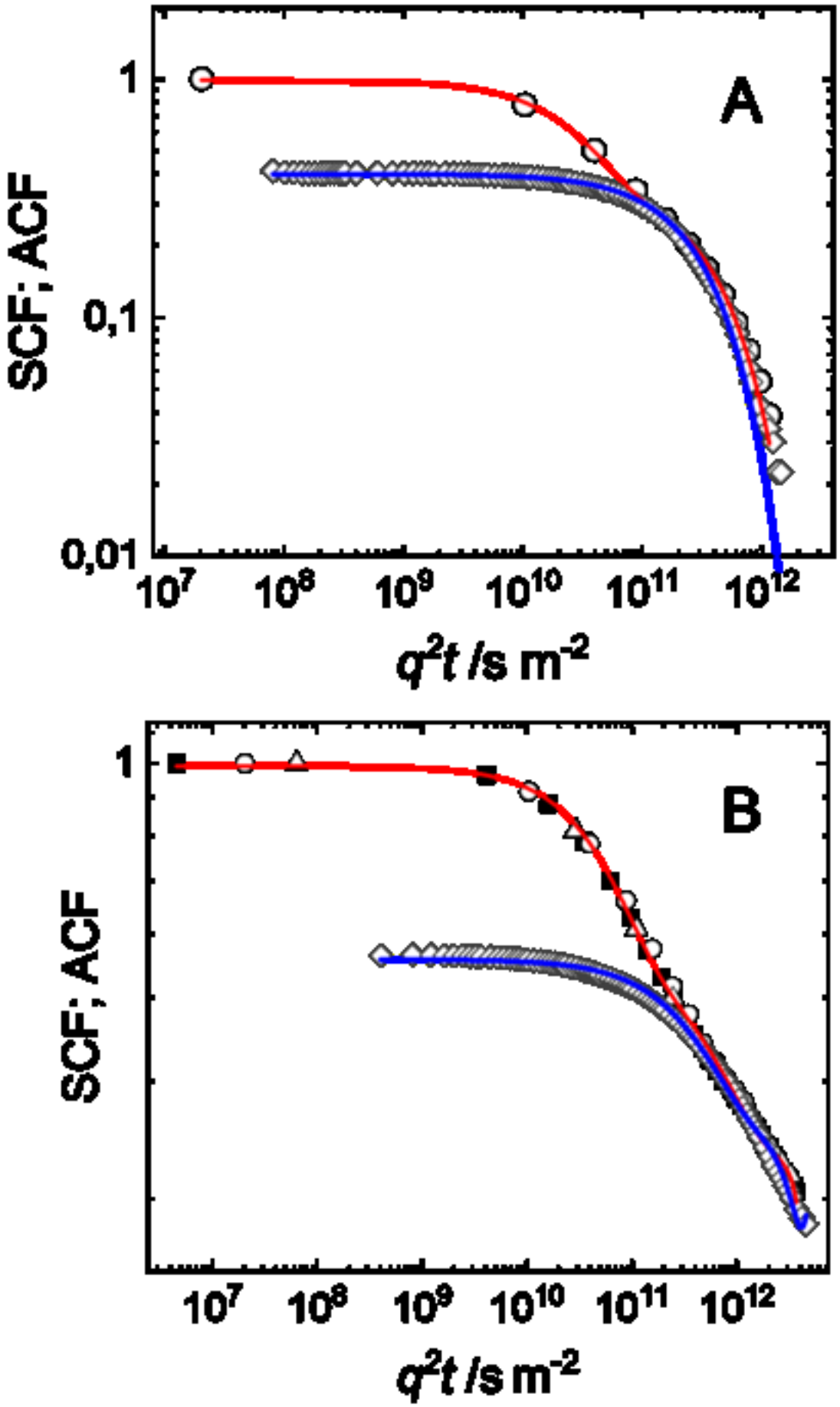

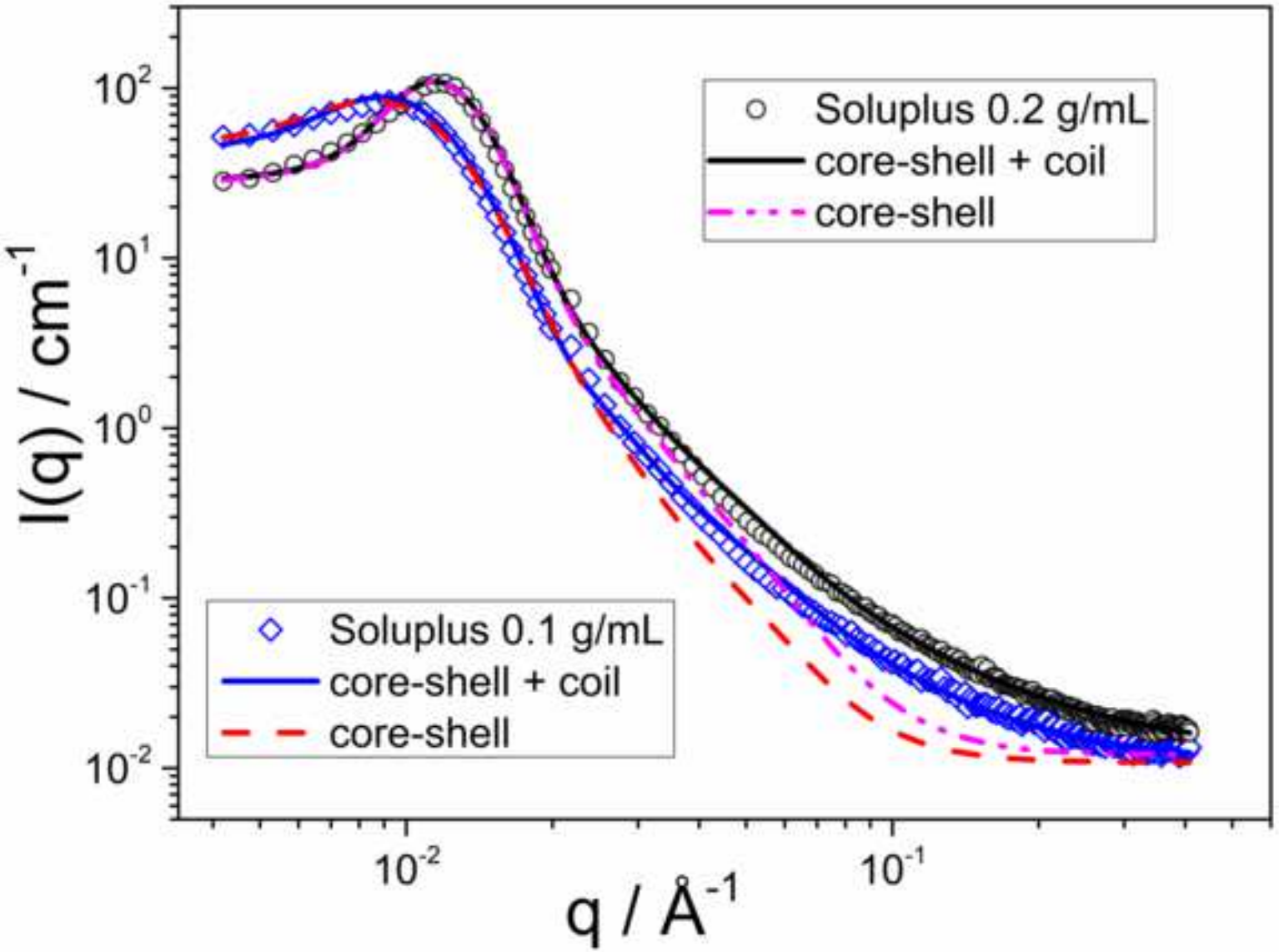

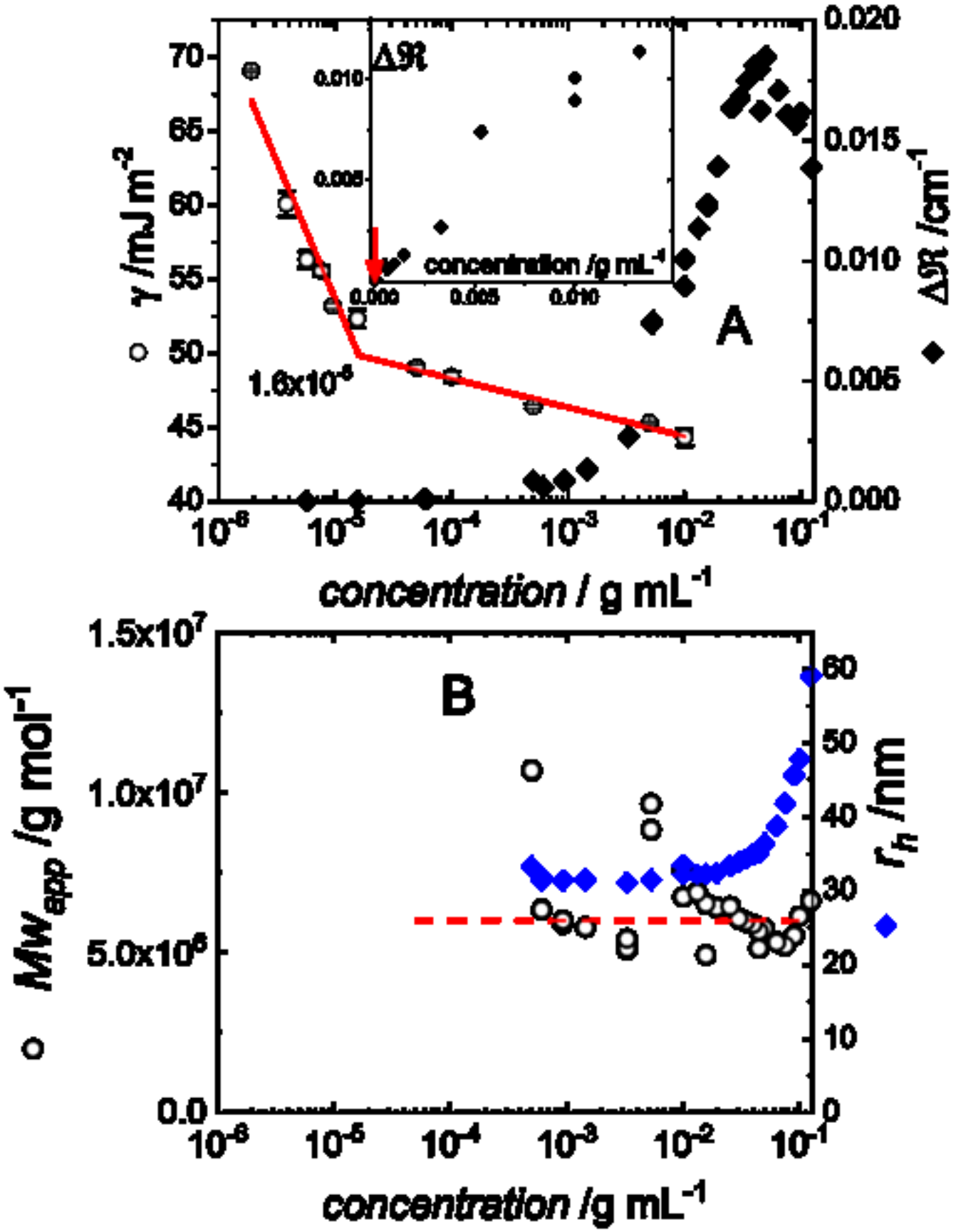

5: Figure 9

Click here to access/download;5: Figure;fig9.tif